

Peer review status:

This manuscript is undergoing peer review at Seismological Research Letters.

This is a non-peer-reviewed preprint submitted to EarthArXiv.

Extremely Shallow Semi-Repeating Tremor

Caused by Water Hammers in a Sewer Pipe

in Social Circle, Georgia

Xu Si^{*1} and Zhigang Peng¹

Abstract

Repeating earthquakes are mostly generated by small asperities that are loaded by continuous creep surrounding them, and their recurrence times are inversely proportional to the loading rates. However, sometimes anthropogenic activities can also produce repeated seismic shakings with shorter recurrence intervals, and their source mechanisms can vary. Here we investigated semi-repeating ground vibrations recorded in Social Circle, Georgia starting on August 14th 2025. Ten tremor-like events were captured by sixteen three-component SmartSolo sensors during one hour on August 15th 2025, followed by four days of continuous observation at three stations. The signals recur nearly every six minutes with similar but not truly repeating waveforms and clear diurnal amplitude variations that are stronger during daytime. Clustering analysis reveals several sub-event types with distinct coda durations. Their timing correlates with expected residential water-use patterns, suggesting a shallow anthropogenic source. Later excavations revealed that a forced main pipe connected to a local pump station vibrated nearly every six minutes, likely caused by the water hammer effect due to a faulty check valve. These findings demonstrate that human activities in the shallow subsurface can generate semi-repeating seismic waves, exhibiting recurrence behavior analogous to natural fault or volcanic systems. Correctly identifying their causes help to better distinguish them from naturally occurring events.

Cite this article as Si X. and Z. Peng (2025). Extremely Shallow
Semi-Repeating Tremor Caused by Water
Hammers in a Sewer Pipe in Social
Circle, Georgia, *Seismol. Res. Lett.* XX,
1–20, doi: 00.0000/000000000.

Supplemental Material

^{1.} School of Earth and Atmospheric Sciences, Georgia Institute of Technology, Atlanta, GA, USA,

^{*}Corresponding author: xsi33@gatech.edu

Introduction

In recent years, seismometers have been increasingly used not only to record natural earthquakes but also to monitor a wide
range of anthropogenic and environmental activities (also known as environmental seismology) (Larose et al., 2015). For
example, global lockdown during the COVID-19 pandemic provided a unique opportunity to observe sharp reductions in
anthropogenic seismic noise in cities around the world (Lecocq et al., 2020; Poli et al., 2020; Xiao et al., 2020). Similar seismic instruments have been applied to detect oceanic microseisms (Ardhuin et al., 2011), atmospheric disturbances (Nishida,
2017) such as winds (Johnson et al., 2019) or extreme weather events (Ebeling and Stein, 2011), and to identify car traffic (Diaz
and Schimmel, 2017), train movements (Fuchs et al., 2018; Li et al., 2018; Maher et al., 2025), airplanes and helicopters (Meng
and Ben-Zion, 2018), holiday activities (Wang et al., 2020; Chu et al., 2024), and other industrial vibrations (Green et al.,
2020) in densely populated areas. These examples highlight the expanding role of seismology in monitoring near-surface
processes and human-environment interactions beyond traditional earthquake studies. Such interdisciplinary approaches
have transformed sensitive seismic instruments for discrete seismic event observation and continuous environmental monitoring (Diaz, 2016), but also highlight the need to distinguish between naturally and anthropogenically generated seismic
signals (Fernando et al., 2024; Maher et al., 2025).

Repeating earthquakes (also known as repeators) are defined as seismic events that recur at nearly the same location

Repeating earthquakes (also known as repeators) are defined as seismic events that recur at nearly the same location
with similar source properties (Uchida and Bürgmann, 2019). They have been widely applied in tectonic (Nadeau and
Johnson, 1998), volcanic (Massin et al., 2013), and glacial (Danesi et al., 2007) settings, as well as in other tectonic environments (Uchida and Bürgmann, 2019; Cesca et al., 2024). These observations provide valuable information on fault slip
behavior, stress accumulation, and subsurface mechanical properties. Tectonic and glacial repeaters are typically associated
with slip along material interface that rupture quasi-periodically (Beeler et al., 2001), allowing estimates of slip rate and stress
renewal time. While repeaters in volcanic settings often reflect cyclic processes linked to magmatic degassing or hydrothermal
fluid flow, they can also be driven by stick-slip motions (Kendrick et al., 2014). Across these diverse environments, repeating
events demonstrate that seismic energy can be released in a temporally organized manner, governed by the interplay between
stress loading and boundary conditions.

Although most known repeaters are generated by natural processes, near-surface human activities can also produce periodic seismic signals. Anthropogenic sources such as groundwater extraction, fluid injection, pumping systems, ventilation
fans, firworks and heavy machinery may generate repeatable vibrations with distinct temporal patterns (Schwardt et al., 2022;
Fang et al., 2020; Chu et al., 2024). These signals typically have small magnitudes with recurrence characteristics similar to
natural repeaters, and they occur in the air, on the surface, or at very shallow depths. Accurate identification and characterizing of such anthropogenic signals is important to distinguish human-induced vibrations from natural seismicity, improve the
reliability of regular earthquake catalogs, and understand the influence of human activities on shallow subsurface structures.

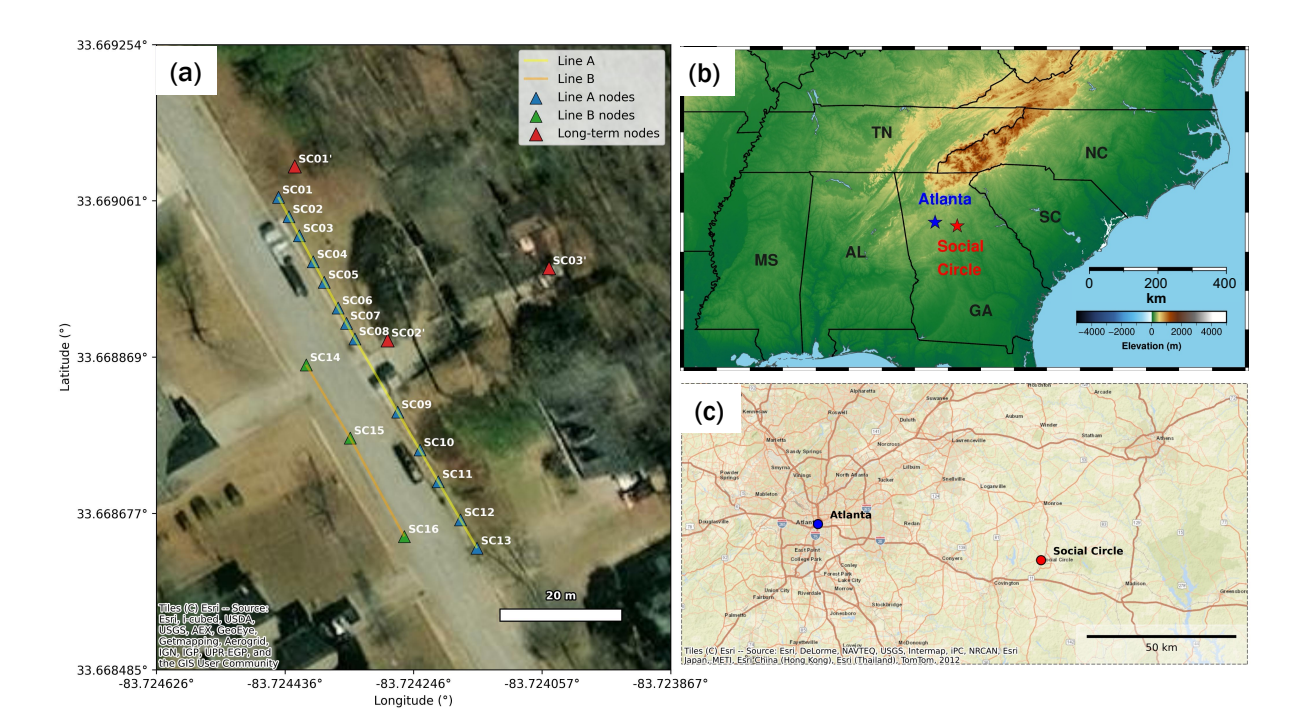


Figure 1. Seismic array deployment and regional setting near Social Circle, Georgia. (a) Local layout of two nodal lines (A and B) and three long-term (one week) nodes. (b) Regional map showing the location of Social Circle (red star) relative to

Atlanta (blue star) within the southeastern United States. (c) Satellite view highlighting the relative positions of Atlanta and Social Circle.

On August 15th 2025, residents of Social Circle, Georgia, reported minor ground shakings with booming sounds that
occurred repeatedly throughout the day, prompting a rapid-response seismic investigation (Fig. 1). To identify the origin
of these signals, we deployed 16 500-Hz SmartSolo sensors of three-components for a continuous recording of one hour
in the affected residential area. Three stations were left to record continuously for the next week. The recordings reveal a
series of highly periodic tremor-like events with a recurrence interval of approximately six minutes. In the next sections, we
briefly described the methods used to detect these events and examined their waveform characteristics. We also attempted
to examine their daily patterns and compare with naturally observing deep tremors to better understand their generation
mechanism.

Observations and Data Collection

- 46 Social Circle is a city in southern Walton County, Georgia, USA, located about 72 km east of Atlanta (Fig 1). In response to
- 47 unusual reports of repeated shaking in this neighborhood and a call from Georgia Emergency Management Agency (GEMA)
- on August 15th 2025, a team from Georgia Institute of Technology conducted a rapid seismic survey using sixteen three-
- 49 component 500 Hz SmartSolo seismometers. The primary objective was to record the signals at high spatial resolution and
- generate a dataset that could be directly compared with eyewitness reports from local residents. Because the phenomenon

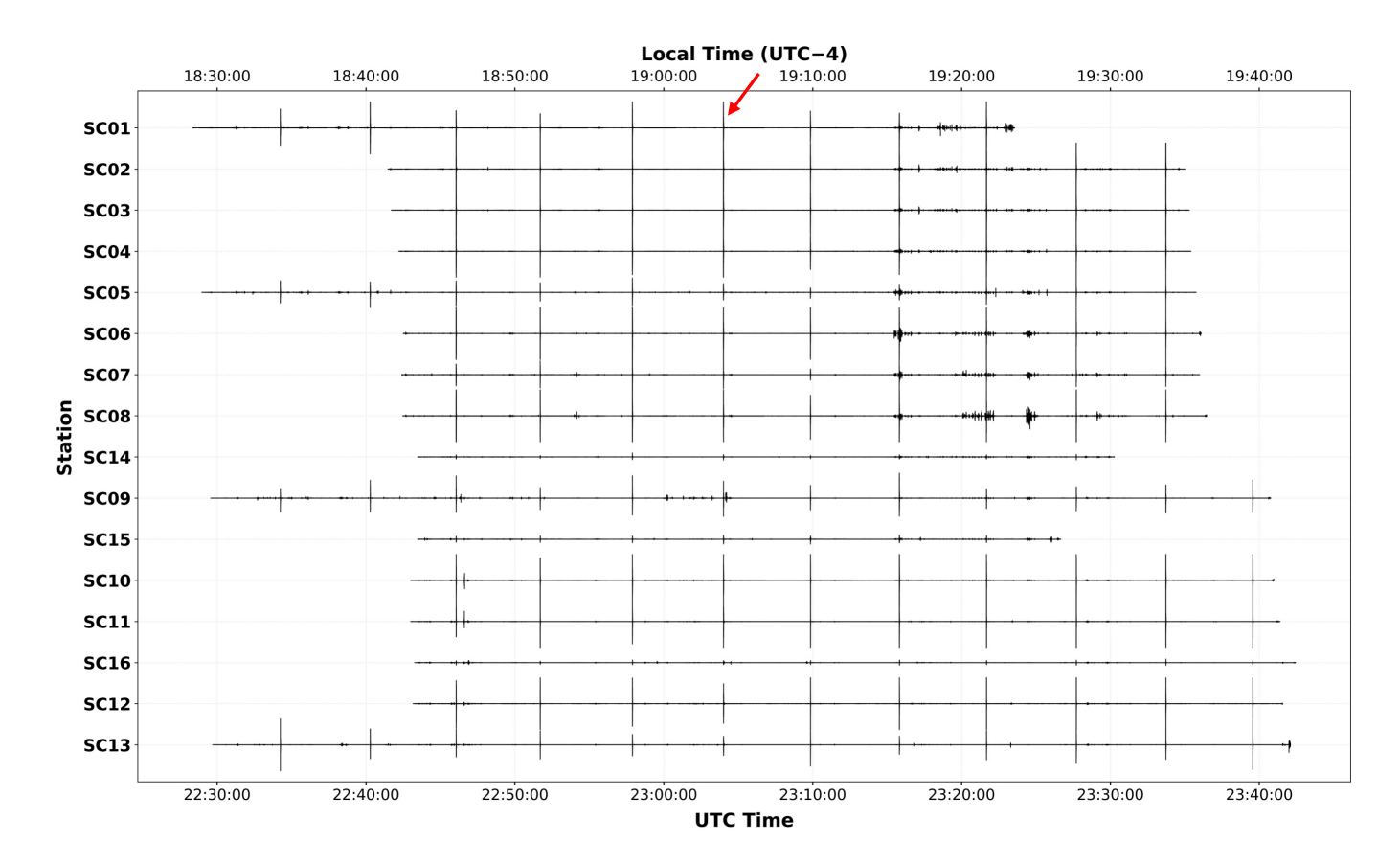


Figure 2. One-hour continuous seismic records from 16 stations deployed along the northwest–southeast line in Social Circle, Georgia. The traces are arranged by station position

along the line (SC01–SC16) and plotted with a uniform vertical offset for clarity.

- was suspected to originate from a shallow and highly localized source, the deployment emphasized dense coverage within
 the neighborhood rather than wider regional spacing.
- The stations named SC01 to SC13 (Line A) were oriented northwest to south east across the affected block and extended 50 m in length, forming the main transect of the array (Fig. 1). SC14 to SC16 (Line B) constituted a shorter parallel transect of 30 m, separated from Line A by approximately 10 m across a local street. Inter-station spacing along both transects ranged from 3 to 10 m. This dense geometry provided sufficient resolution to resolve relative timing and amplitude variations in the affected neighborhood.
- The full sixteen-station array operated for approximately one hour, during which ten repeating events were recorded.
 Following this reconnaissance phase, most of the instruments were removed. For long-term monitoring, three stations
- (SC01', SC02' and SC03') were redeployed at key positions to continuously record for the following 7 days. This two-stage
- deployment strategy, combining dense short-term coverage with sparse but sustained monitoring, enabled us to capture both
- the spatial distribution and temporal evolution of the signals, forming the basis for subsequent analysis of the Social Circle
- 63 sequence.

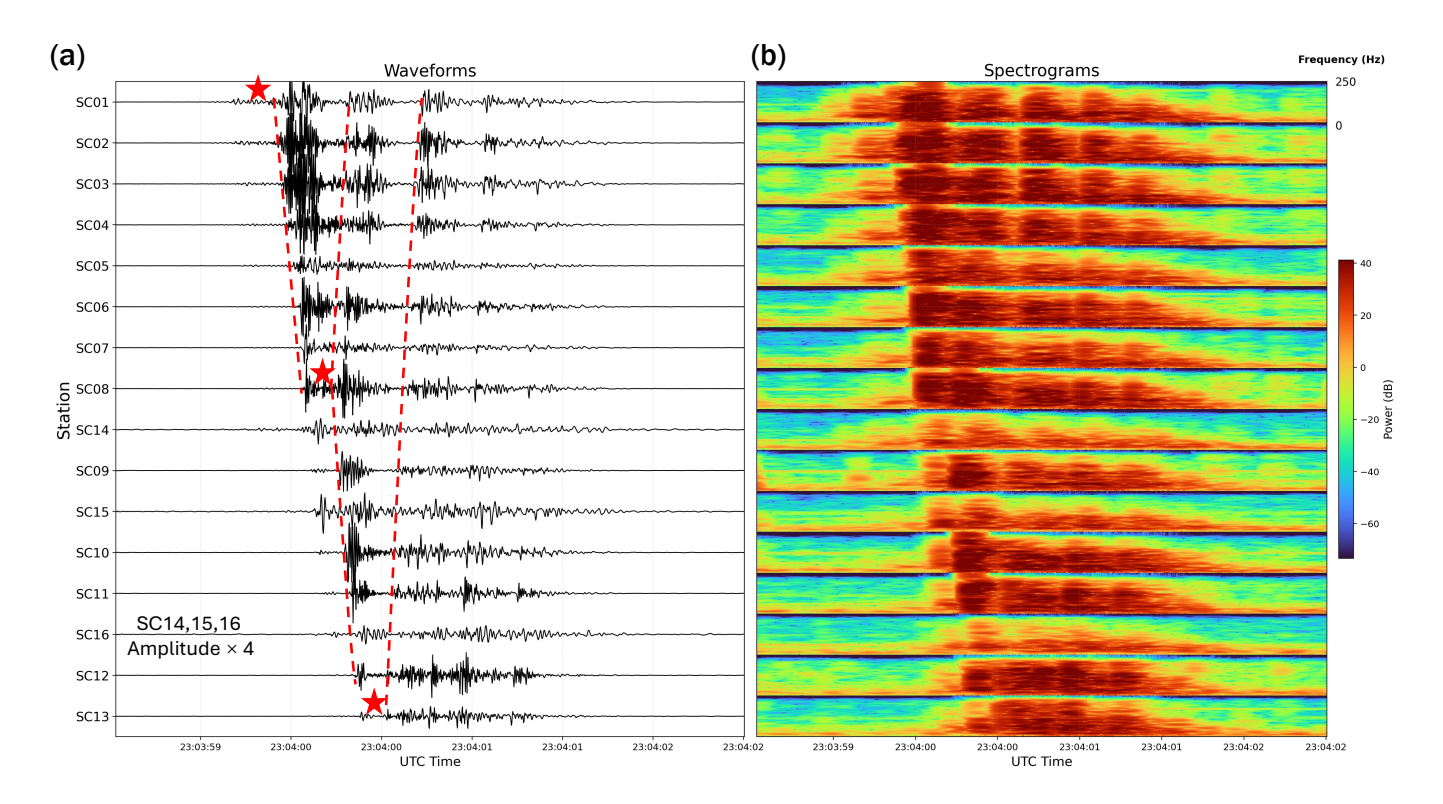


Figure 3. Example of an event recorded during the continuous monitoring phase. (a) Waveform records from the array showing approximately five subevents. Red stars denote the

potential source locations of the first three subevents. (b) Corresponding spectrogram illustrating the frequency content of the event

Results

- 65 One hour monitoring
- During the one-hour continuous recording (from August 15, 22:30 UTC to 23:40 UTC), the 16-station array detected ten clear
- 67 impulsive signals (Fig. 2). Each signal shows coherent onsets and consistent amplitudes across multiple stations. The signals
- were recorded almost simultaneously by both Line A and Line B stations, indicating a common and spatially extended source.
- 69 Their waveforms exhibit stable amplitudes and high signal-to-noise ratios, which makes them easily distinguishable from
- background noises. In addition, these events exhibit a nearly regular time interval of approximately six minutes, indicating
- ⁷¹ a quasi-periodic behavior of the source.
- To further examine the waveform characteristics, we selected one representative event that was recorded by all stations
- ⁷³ (Fig. 3a). This event occurred at approximately 23:04:00 UTC (07:04:00 PM EDT). The amplitudes from Line A stations were
- plotted using a uniform scale, while those from Line B were multiplied by a factor of four for better comparison with the Line-
- A recordings. The corresponding spectrogram (Fig. 3b) showed that this event consists of a series sub-events with gradually
- decreasing energy. The first three sub-events were particularly clear and were marked (Fig. 3a). The sub-events had either
- ⁷⁷ sharp arrivals (e.g., ev1 at SC07 and SC08), or tremor-like signals with spindle shapes (e.g., ev1 and ev2 at SC02 SC03). The
- 78 relative arrival times indicate that the source propagated from northwest to southeast across the array, with an apparent
- velocity of about 100 m/s. Such a propagation pattern suggests an extremely shallow and moving source process.

80 Four days monitoring

In addition to the one-hour dense-array recording, we examined a four-day interval to evaluate the temporal variability and persistence of the observed signals. Figure 4 presents four consecutive days of continuous waveform and the corresponding envelope at station SC02′ (N component). The signals were detected using a standard peak-detection algorithm (Duarte, 2021) applied consistently throughout the analyzed time period. The detected times aligned well with visually discernible onsets, demonstrating the robustness of the detection procedure under varying background conditions. In addition, the corresponding E and Z components at SC02′, as well as all three components at SC01′, were provided in the Supplementary Material and showed consistent behavior. Waveforms recorded by station SC03′ were excluded from this analysis due to their weak signal-to-noise ratios, which prevented reliable detection.

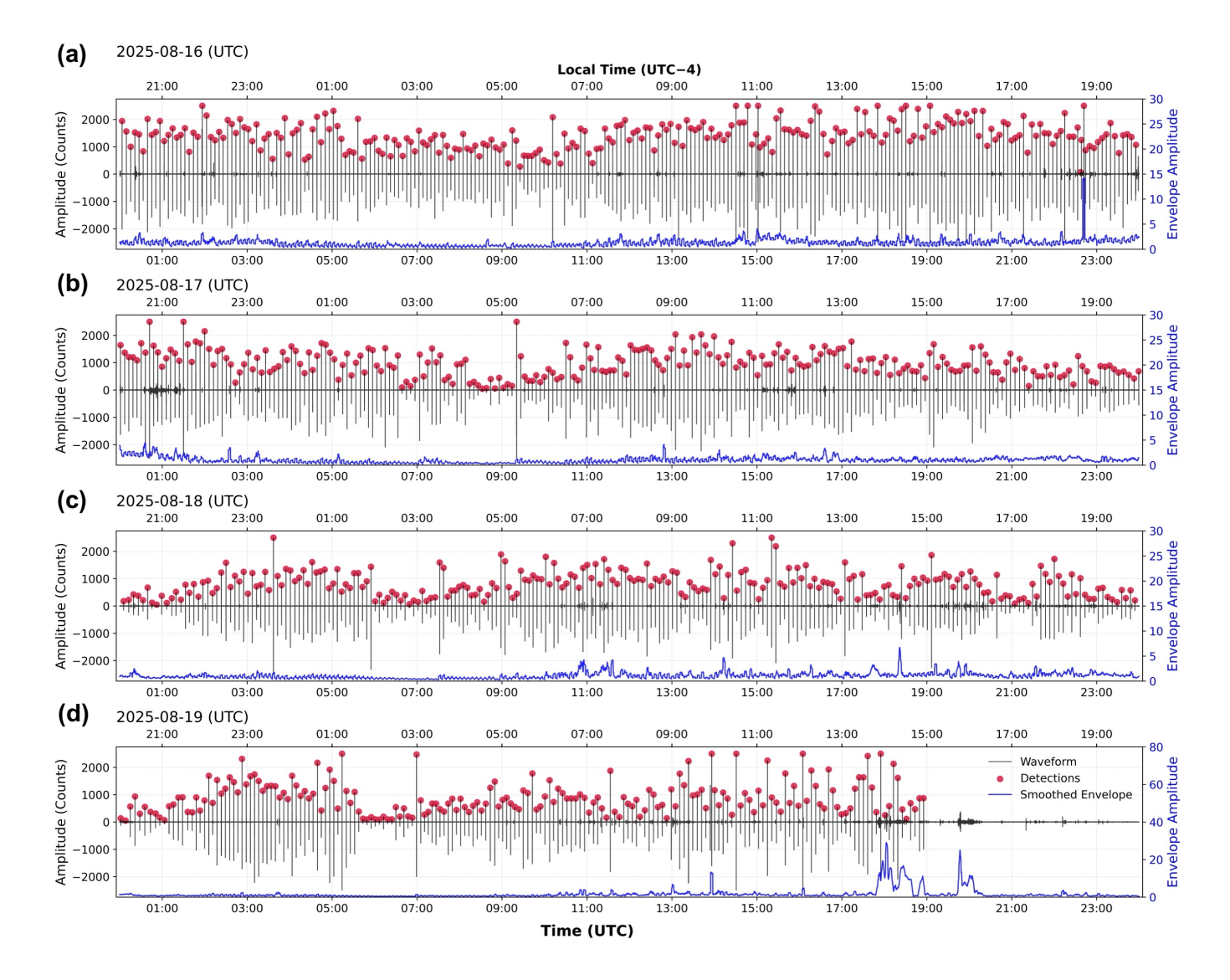


Figure 4. Continuous waveform and detection results at station SC02' (E component). The black line represents the raw waveform, while the blue curve shows the smoothed envelope (10-minute moving window), which reflects the

background amplitude variation. The detection algorithm identified a sequence of repeating events (red dots) from 16 August to 19 August 2025, with the last event occurring around 15:00 local time (UTC+4).

While exceptionally low-amplitude events may remain below the detection threshold, the frequent occurrence of identified signals and their clear visibility in the continuous waveform record suggest that, in a broad statistical sense, the vast majority of events during this period were successfully captured. This provides a robust basis for computing the hourly statistics of event amplitudes (Fig. 5) and inter-event times (Fig. 6).

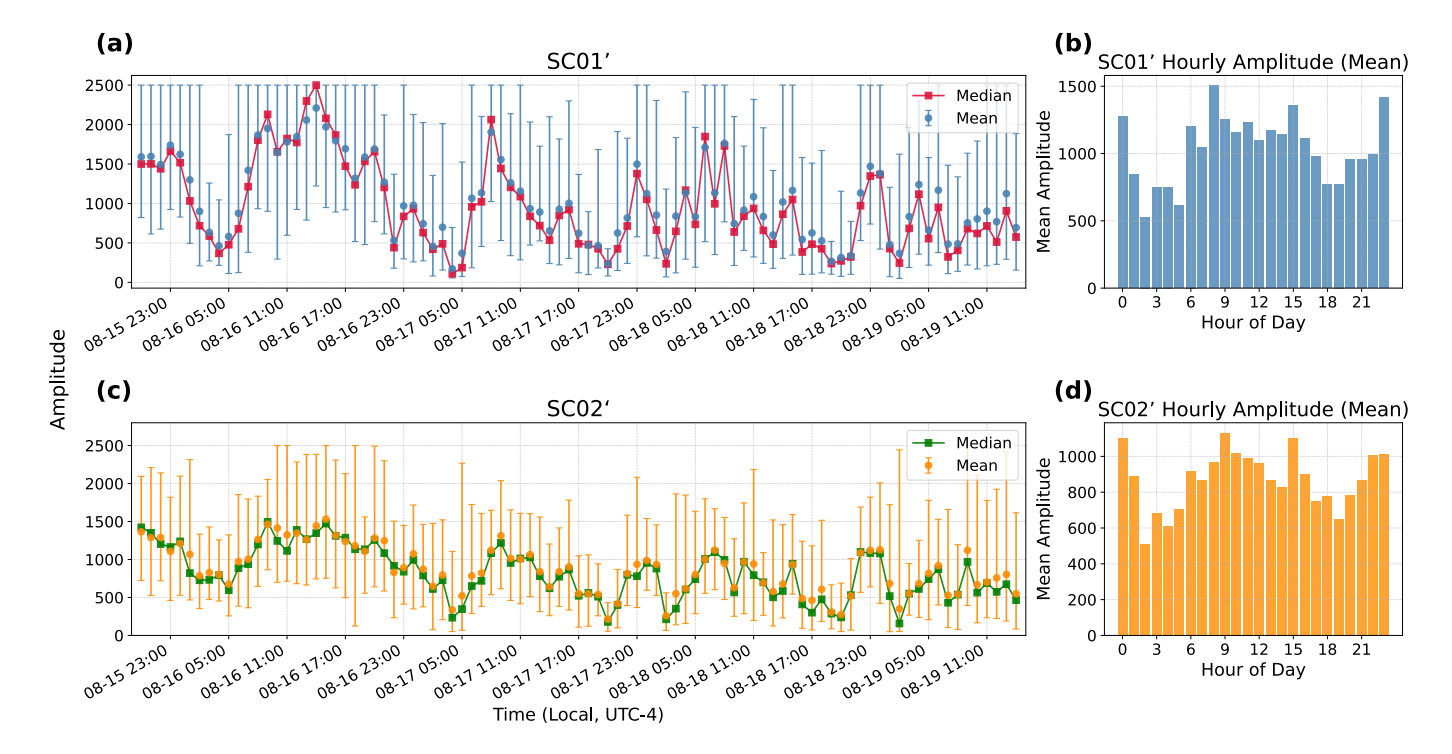


Figure 5. Hourly statistics of event amplitudes at two high–signal-to-noise ratio stations, SC01' and SC02', during 16–19 August 2025. For each station, the amplitudes of the three components were averaged to obtain a representative value. (a) Modified boxplot of hourly amplitudes for SC01', showing minimum, maximum, mean (blue), and median (red). (b) Histogram of hourly mean amplitudes for SC01', where the x-axis represents the hour of the day and the y-axis gives the

aggregated mean amplitude across the four-day monitoring period. (c) Modified boxplot of hourly amplitudes for SC02', showing minimum, maximum, mean (orange), and median (green). (d) Histogram of hourly mean amplitudes for SC02', with the same axis definitions. Together, these results highlight both the temporal variability and the distribution of event amplitudes at the two stations.

Next, we computed the distribution of signal amplitudes in hourly bins (Fig. 5) and summarized each bin by both the mean and the median. The two summary metrics yield consistent results and reveal a pronounced diurnal cycle. For example, on Saturday 16th August 16th, the amplitudes during the daytime hours are systematically larger than during the subsequent early-morning period. A clear minimum occurred during 01:00–05:00 EDT on Sunday August 17th, where both the mean and the median exhibit their lowest values of the day. The corresponding histogram views (Fig. 5 b and d) reinforce this pattern: the hourly amplitude distributions contract and shift to lower values during the early-morning window, and broaden toward higher values during daytime. This day-to-night contrast repeats over multiple days in the record of several days and is present at both stations, indicating that the diurnal modulation is not station-specific.

To characterize the temporal spacing of the detections, we also computed the Inter-Event Times (IETs) as the time differences between successive detections and aggregated them in hourly bins (Fig. 6). To mitigate undue influence from sporadic

101

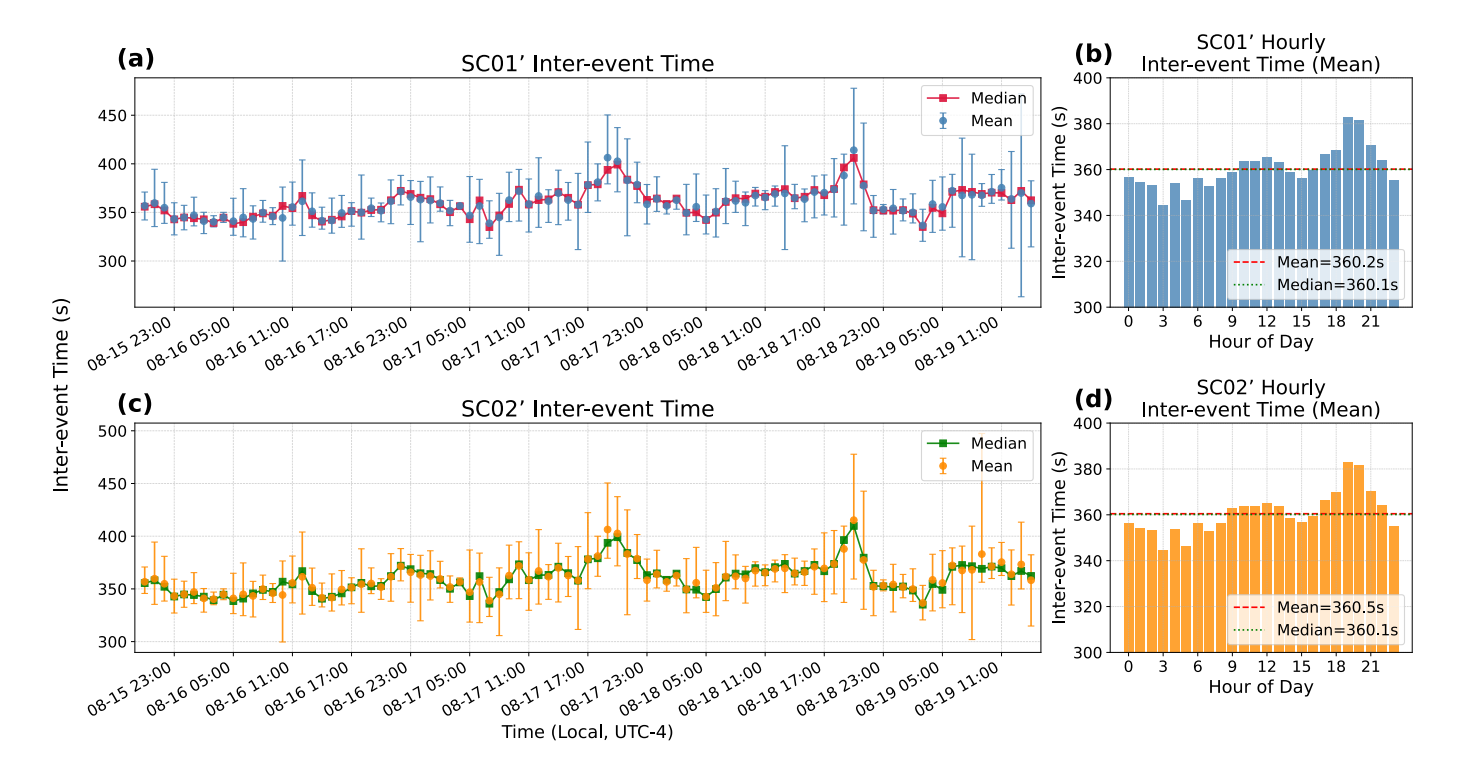


Figure 6. Hourly statistics of inter-event times at two high–signal-to-noise ratio stations, SC01' and SC02', during 16–19 August 2025. The inter-event time is defined as the time interval between two consecutive detections, measured in seconds. (a) Modified boxplot of hourly inter-event times for SC01', showing minimum, maximum, mean, and median values. (b) Histogram of hourly mean inter-event times for

SC01', where the x-axis represents the hour of the day and the y-axis gives the aggregated mean inter-event time across the four-day monitoring period. (c) Modified boxplot of hourly inter-event times for SC02'. (d) Histogram of hourly mean inter-event times for SC02'. The overall mean and median values are close to 360 s (6 minutes), consistent with the repeating nature of the detected sequence.

long gaps, we removed a small number of outliers with IET > 600 s prior to summarizing. This trimming does not affect the main features described below. Over the 4 days, the overall mean IET is close to 6 min (\approx 360 s). Superimposed on this baseline, Fig. 6 also reveals a clear diurnal pattern: between 00:00 and 06:00 EDT, the hourly mean IET is systematically below 360 s, indicating more closely spaced detections; during daytime hours, the hourly mean IET is consistently above 360 s, indicating more widely spaced detections.

To summarize the observations so far, we found that amplitudes exhibit a day–night contrast with lower values in the early-morning window and higher values during daytime, whereas inter-event times show an inverse pattern, with shorter spacing overnight (mean < 360 s between 00:00–06:00) and longer spacing during the day (mean > 360 s). These patterns appear in both mean and median amplitude metrics across two stations, and persist after removing a small fraction of long-gap outliers in the IET calculation. Together, they indicate a repeatable and time-of-day–dependent modulation of both signal size and occurrence rate over the 4 days.

Events waveform analysis

After detecting events within the four days of continuous recording, a total of 913 events were identified. For each event in SC01′, three-component waveforms were extracted using a 2.4 s time window (1.0 s before and 1.4 s after the detection

103

104

105

106

108

109

110

111

112

113

time). We then computed the spectrogram of each waveform and applied the seismological foundation model (Si et al.,
2024) to extract high-level spectral features. These features were subsequently reduced in dimensionality using the t-SNE
method (Maaten and Hinton, 2008) for visualization and clustering (Figure 7). Events in Cluster 6 exhibit strong temporal
coherence, occurring predominantly between 0:00 and 6:00 AM local time. The other clusters do not have any particular
occurrence patterns.

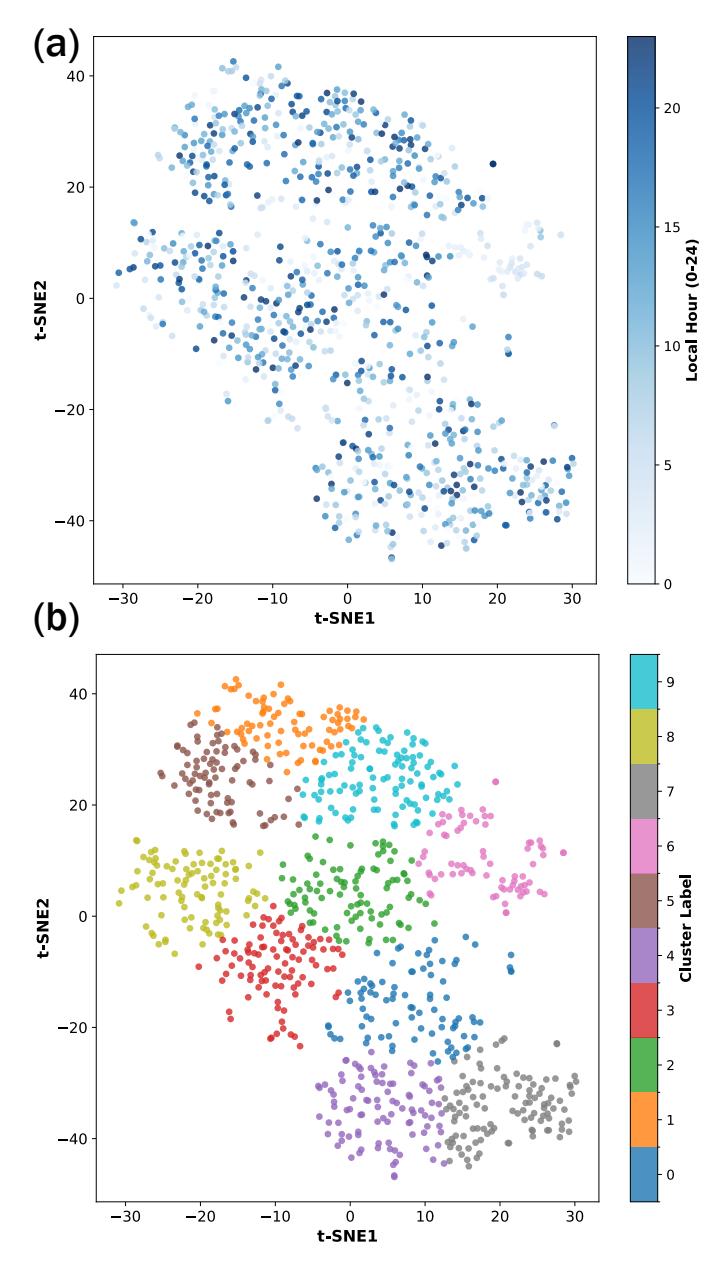


Figure 7. Event feature representation and clustering results based on four days of continuous detections. (a) t-SNE projection of all 913 detected events, color-coded by local hour (0–24). (b) t-SNE projection with color-coded cluster labels showing seven distinct groups obtained from unsupervised clustering. The clustering results indicate that events with similar spectral characteristics tend to occur during comparable local times, suggesting temporal patterns in source or coupling behavior.

To further investigate the relationships among different clusters, we calculated the cross-correlation between all events.

Figure 8a displays the resulting correlation matrix, sorted according to cluster assignment, whereas Figure 8b presents a

122

zoom-in view of Cluster 6. Notably, strong correlation coefficients are observed only within Cluster 6, indicating a high value of waveform similarity among these events.

To illustrate this more clearly, we selected two representative events and plotted their 20 most highly correlated events on the vertical (Z) component before and after waveform alignment. Nearly all of these events belong to Cluster 6, and many exhibit strikingly similar waveforms. The results reveal that these events generally have very short durations (0.05 s) of the primary arrivals and no additional reverberations. These observations suggest that, although the signals repeat at roughly 6-minute intervals, they are not perfectly identical, i.e., not truly repeating earthquakes (Uchida, 2019). Some events exhibit relatively short codas, while others may contain multiple overlapping events within individual recordings (shown in Fig. 3). Each occurrence exhibits distinct variations in waveform shape, coda length, and signal energy.

Vibrating Source

126

127

130

131

132

Our analysis so far was able to characterize nearly repeated natures of the IETs, and potential migrating sources with an apparent speed of 100 m/s (Fig. 3). Such a migration speed is a few times faster than the 30-200 km/hr (8-56 m/s) fast 135 migration speed of low-frequency earthquakes during deep tectonic tremor at major plate boundary zones (Ghosh et al., 136 2010; Shelly et al., 2011). To compare them further, were we showed a zoom-in plot of waveforms recorded in Social Circle 137 (Fig. 3) a triggered tremor recorded along the Parkfield-Cholame section of the San Andreas Fault in Central California 138 (Fig. 9). The tremor was triggered by the surface waves of the 2002 Mw 7.8 Denali Fault earthquake in Alaska ((Peng et al., 139 2009)). Although the amplitude scales and overall frequency ranges differ between the two cases, the spectrograms display 140 qualitatively similar repeating patterns in the time-frequency domain, highlighting the resemblance between the Social Circle signals and the tectonic triggered tremor. However, we were unable to uniquely identify the exact source of these tremor-like signals. Nevertheless, we did present our preliminary analysis results to GEMA, and pointed out the similarities 143 between the observed signals here and the deep tectonic tremor observed at major plate boundary zones (Peng et al., 2009; 144 Peng and Gomberg, 2010). We also proposed a tentative mechanism where shallow groundwater flows were temporally 145 clogged, resulting in a water-hammer effect that has been invoked to explain deep tectonic tremor (Yin, 2018). 146

These efforts partially motivated local emergency responders to perform ground penetrating radar (GPR) survey and subsequent excavation in the area where repeated vibrations occurred. A section of a force main pipe was exposed during excavation on August 19th 2025, and visible movement of the pipe was observed during the ground vibration, confirming the cause (Jonathan Jones@GEMA, personal communication August 19th 2025). A faulty check valve on a pump station within the local sewer infrastructure was later identified, which generated water hammers and ground vibrations once every 6 minutes (Fig. 10). Once the pump was turned off on 3 pm EDT August 19th 2025, the repeated tremor disappeared (Fig. 4).

147

149

150

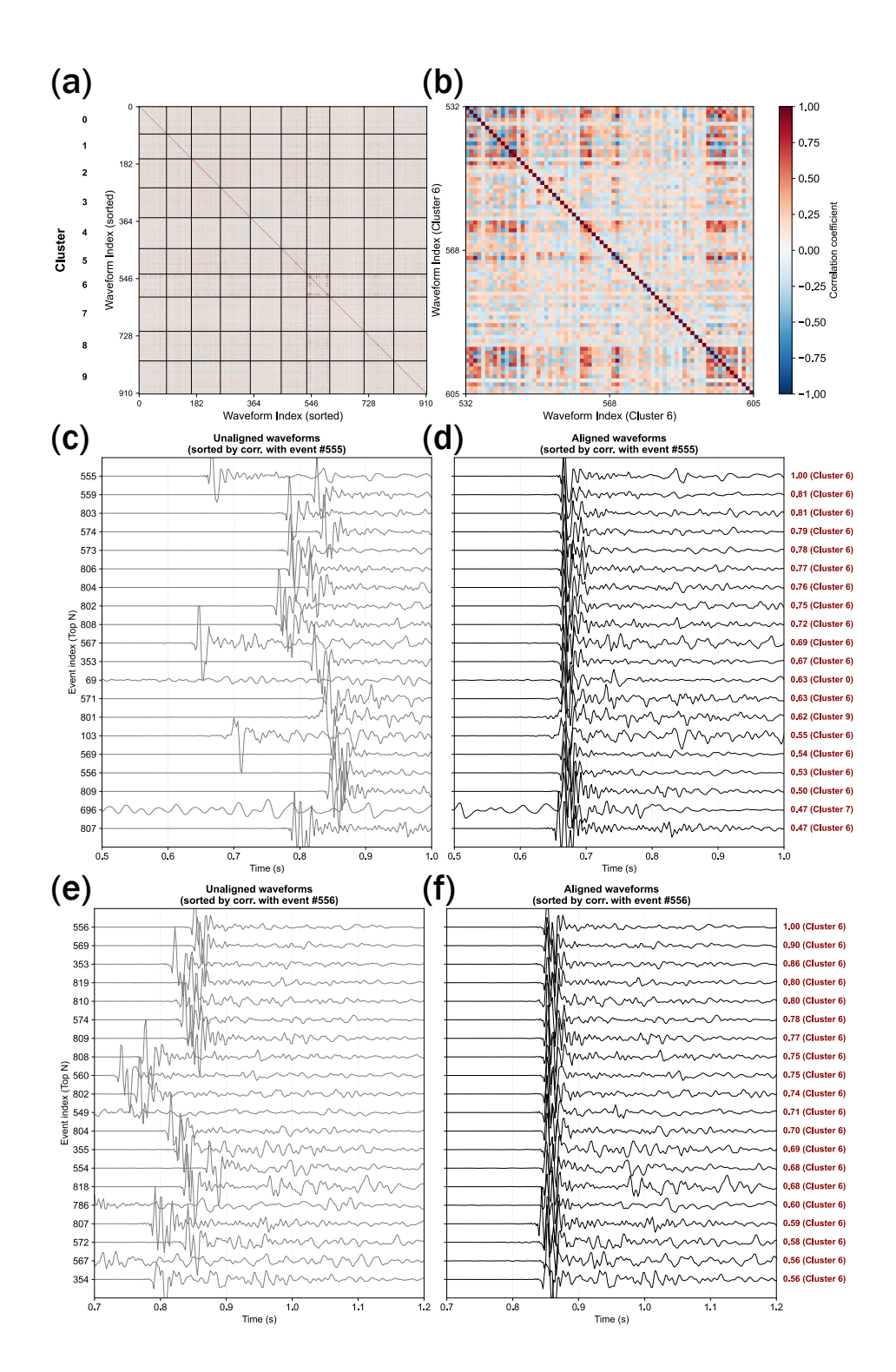


Figure 8. Waveform alignment and comparison of clustered events. (a) Cross-correlation matrix of all events, sorted by cluster assignment. (b) Zoom in view of Cluster 6, showing that strong correlation coefficients are concentrated only within this cluster. (c–f) Examples of two representative reference events (555 and 556) and their 20 most highly correlated events on

the vertical (Z) component. Panels (c) and (e) display the unaligned waveforms, whereas panels (d) and (f) show the corresponding aligned traces. The left y-axis represents the event ID, while the right y-axis indicates the correlation coefficients with the reference events and their corresponding cluster labels.

Discussion

155

The events recorded in Social Circle represent a special type of anthropogenic repeaters. These events are generated by sewer

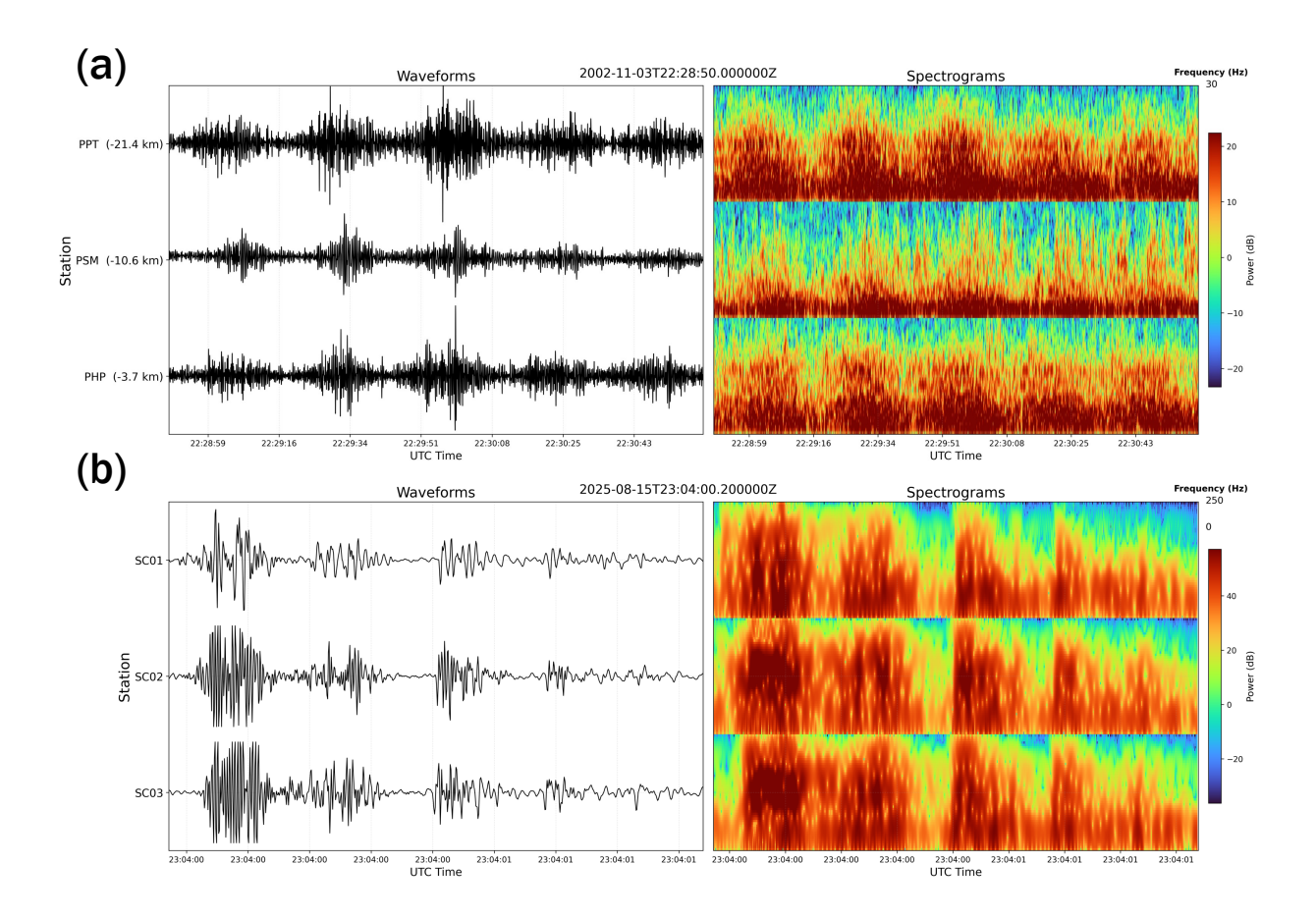


Figure 9. Waveform and spectrogram comparison between the Social Circle event and a triggered tremor in San Andreas Fault during the 2002 Mw 7.8 Denali earthquake. (a) Records of triggered tremor form the stations along the San Andreas Fault during the 2002 Mw 7.8 Denali Earthquake (data similar

to Figure 3 in Peng et al. (2009)), with waveforms band-pass filtered between 2–8 Hz. The spectrograms show the characteristic long-duration and low-frequency energy pattern associated with tremor. (b) Zoom-in view of three stations (SC01, SC02, SC03) from the Fig. 3.

tics of these signals show a strong correlation with residential water usage. Although the pipe belongs to the sewer system, its vibration pattern is expected to reflect the temporal variability of household water consumption. As shown in the evolution of the mean hourly water demand during a typical 24-hour period (Herrera et al., 2010), two pronounced minima appear: (1) between 1 a.m. and 5 a.m., corresponding to residents' sleeping hours, and (2) around dinner time (6–7 p.m.). These low-usage periods are consistent with our observation (Fig. 5), indicating that the event amplitude is positively correlated with the expected water volume flowing through the pipe.

Combined with field observations in the study area and the information provided by GEMA, we confirmed that these repeating events are caused by the faulty check valve. The pump station is located at a relatively low elevation, while the pipeline rises slightly toward the observation area. This pipeline is classified as a forced main pipe, meaning that water is pumped from the lower storage tank to a higher outflow pipe by the pump station. In this case, when the check valve malfunctions, water hammer can occur and cause strong vibrations in the pipeline (Ghidaoui et al., 2005; Jung et al., 2009). In the Social Circle case, this mechanism helps explain why the signal amplitude correlates with human water usage, because the

158

159

160

161

162

164

165

166

phenomenon depends on water volume. When the water demand and flow volume increase, the amplitude becomes larger.

Conversely, when residential water demand decreases, the amplitude reduces (Fig. 5). However, the relationship between
amplitude and inter-event time still requires further investigation. More detailed verification will require operational records
from the local sewer facility, which we plan to analyze in the next step.

We note that this phenomenon is not limited to engineered pipeline systems. A magma hammer effect is invoked to explain similar seismic subevents observed at the beginning of the 2022 phreatoplinian Hunga Tonga-Hunga Ha'apai eruption (Zheng et al., 2023). Similar water hammer-like tremors potentially occur at the seismic-aseismic transition zone along major plate boundaries (Yin, 2018). Similarly, transient pressure surge in a fluid-filled fracture at depth can generate seismic waves, which have been invoked to explain remotely triggered seismicity and geothermal or volcanic regions (Brodsky et al., 2003; Zheng, 2018). Taken together, these types of hydraulic transients could also possibly be considered a special type of seismic source in geological systems, such as volcanoes and glaciers (St. Lawrence and Qamar, 1979; Winberry et al., 2009).

Properly identifying the anthropogenic semi-repeating tremor helps to ensure that such signals are not erroneously identified as naturally occurring events (Fernando et al., 2024; Maher et al., 2025). Furthermore, these events provide us with a new
perspective for understanding the source mechanism of naturally occurring repeating earthquakes (Uchida and Bürgmann,
2019). In contrast to natural tectonic (Nadeau and Johnson, 1998; Matsuzawa et al., 2004; Dreger et al., 2007) or volcanic
repeaters (Aster et al., 2008; Park et al., 2019) that originate from fault slip or magmatic processes, the repeating signals
observed at Social Circle, Georgia, are clearly driven by human activity. Their short recurrence interval of approximately six
minutes, shallow source depth, and temporal correlation with local water-use patterns indicate that they result from surface
or near-surface mechanical responses to anthropogenic forcing.

Different from these social circle repeaters that have less similar waveforms but very similar recurrence intervals, those generated by fault slip, glacier motion (Zoet et al., 2012; Paul Winberry et al., 2013; Lipovsky and Dunham, 2016), or magmatic processes (Matoza et al., 2009) usually exhibit extremely high similar waveforms but variable recurrence times. This variability reflects the complexity of stress accumulation and release in natural systems, which are influenced by factors such as overall loading rates and frictional properties. Moreover, because most previous studies identify repeaters using strict correlation thresholds in template-matching analyses, events with relatively stable recurrence intervals but distinct waveform characteristics (like those observed in this study) may have been overlooked. A detailed investigation of such events could provide valuable insights into how repeating seismic signals evolve under varying boundary conditions and external forcing. Nevertheless, several limitations exist in this study. The short monitoring period (four days) limits our ability to capture the long-term or seasonal variability of these anthropogenic repeaters. In addition, the small number of available stations and the nearly linear array geometry prevented us from accurately locating the sources. With the seismic observations alone, we were unable to pinpoint the exact source mechanisms for the repeated tremors. This highlights the need to combine seismic with other geophysical and direct observations to better understand the source processes of earthquake sequences (Shelly, 2024;

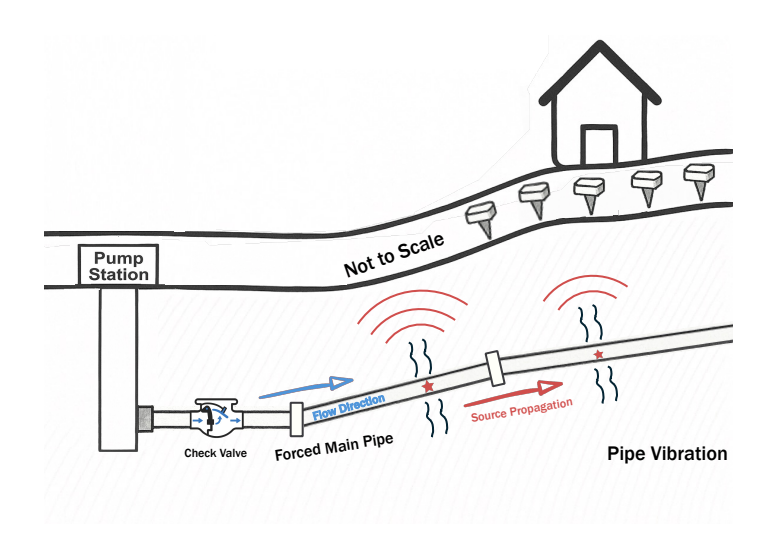


Figure 10. Schematic illustration of the proposed event generation model. Vibrations originate along underground sewer pipes, likely triggered by flow disturbances or pressure fluctuations near the pump station.

Peng and Lei, 2025). Future studies employing dense distributed acoustic sensing (DAS) arrays (e.g., Lindsey and Martin 2021; Zhan 2020), along with other environmental and audio/video recordings would enable higher-resolution imaging of the source process and help clarify the coupling between human activities and surface/near-surface seismic responses.

Conclusion

The seismic observations in Social Circle, Georgia, reveal a series of highly periodic tremor-like events with a recurrence interval of approximately six minutes. These signals exhibit consistent timing and clear diurnal variations in amplitude. Field observations and statistical analyses indicate that the source is anthropogenic, most likely related to the operation of a local sewer pipeline system driven by periodic pumping cycles. The repeating nature and extremely shallow origin of these events confirm that near-surface infrastructure can produce detectable quasi-periodic seismic signals. This study demonstrates that rapid, short-term seismic monitoring can effectively identify and characterize human-induced vibrations in residential environments. Although distinct in physical origin, these anthropogenic repeaters share similar properties of periodic energy release with tectonic or magmatic repeaters, illustrating that repeating seismic behavior can emerge across a wide range of scales and driving mechanisms.

213 Data and Resources

All data used in this study were recorded by the 500 Hz SmartSolo nodal sensors deployed in the Social Circle experiment.

The code for the foundation model, along with the cut waveforms of the 913 events and the one-hour waveform dataset used for analysis, is publicly available at: https://github.com/sixu0/SeisCLIP.1

¹A detailed example illustrating the procedure for extracting spectrogram-based features will be made available in a forthcoming release.

217 Declaration of Competing Interests

The authors acknowledge that there are no conflicts of interest recorded.

219 Acknowledgments

- 220 We thank the Georgia Emergency Management and Homeland Security Agency (GEMA), especially Mr. Jonathan Jones, for coordinating
- the seismic deployment, providing essential information to confirm the source, and offering field support during the investigation. We
- thank Xia Zhu for insightful discussions on water hammer processes, which helped improve the schematic diagram (Figure 10). Finally,
- 223 we sincerely appreciate local residents of Social Circle for their support and allowing the temporary deployment of seismic instruments in
- 224 their community.

225 References

- 226 Ardhuin, F., E. Stutzmann, M. Schimmel, and A. Mangeney (2011). Ocean wave sources of seismic noise. Journal of Geophysical Research:
- 227 Oceans 116(C9).
- Aster, R., D. Zandomeneghi, S. Mah, S. McNamara, D. Henderson, H. Knox, and K. Jones (2008). Moment tensor inversion of very long
- period seismic signals from strombolian eruptions of erebus volcano. Journal of Volcanology and Geothermal Research 177(3), 635–647.
- Beeler, N., D. Lockner, and S. Hickman (2001). A simple stick-slip and creep-slip model for repeating earthquakes and its implication for
- microearthquakes at parkfield. Bulletin of the Seismological Society of America 91(6), 1797-1804.
- 232 Brodsky, E. E., E. Roeloffs, D. Woodcock, I. Gall, and M. Manga (2003). A mechanism for sustained groundwater pressure changes induced
- by distant earthquakes. Journal of Geophysical Research: Solid Earth 108(B8).
- cesca, S., P. Niemz, T. Dahm, and S. Ide (2024). Anti-repeating earthquakes and how to explain them. Communications Earth &
- 235 Environment **5**(1), 158.
- ²³⁶ Chu, R., Q. Wang, Z. Peng, M. Sheng, Q. Liu, and H. Chen (2024). Fireworks: A potential artificial source for imaging near-surface
- structures. Seismological Research Letters **95**(1), 435–447.
- Danesi, S., S. Bannister, and A. Morelli (2007). Repeating earthquakes from rupture of an asperity under an antarctic outlet glacier. Earth
- 239 and Planetary Science Letters **253**(1-2), 151–158.
- 240 Díaz, J. (2016). On the origin of the signals observed across the seismic spectrum. Earth-Science Reviews 161, 224–232.
- 241 Dreger, D., R. M. Nadeau, and A. Chung (2007). Repeating earthquake finite source models: Strong asperities revealed on the san andreas
- fault. Geophysical Research Letters 34(23).
- Duarte, M. (2021, March). detecta: A python module to detect events in data.
- 244 Díaz, J. and M. Schimmel (2017). Seismometers within cities: Worldwide observations of urban seismic noise. Seismological Research
- 245 Letters 88(3), 899–907.
- Ebeling, C. W. and S. Stein (2011). Seismological identification and characterization of a large hurricane. Bulletin of the seismological
- society of America **101**(1), 399–403.
- Fang, G., Y. E. Li, Y. Zhao, and E. R. Martin (2020). Urban near-surface seismic monitoring using distributed acoustic sensing. Geophysical
- Research Letters **47**(6), e2019GL086115.

- Fernando, B., P. Mialle, G. Ekström, C. Charalambous, S. Desch, A. Jackson, and E. K. Sansom (2024). Seismic and acoustic signals from
 the 2014 'interstellar meteor'. *Geophysical Journal International* **238**(2), 1027–1039.
- ²⁵² Fuchs, F., G. Bokelmann, and A. W. Group (2018). Equidistant spectral lines in train vibrations. Seismological Research Letters 89(1), 56–66.
- ²⁵³ Ghidaoui, M. S., M. Zhao, D. A. McInnis, and D. H. Axworthy (2005). A review of water hammer theory and practice. *Appl. Mech. Rev.* **58**(1),
- 254 49-76.
- Ghosh, A., J. E. Vidale, J. R. Sweet, K. C. Creager, A. G. Wech, H. Houston, and E. E. Brodsky (2010). Rapid, continuous streaking of tremor
- in cascadia. Geochemistry, Geophysics, Geosystems 11(12).
- Green, R. G., I. D. Bastow, and B. Dashwood (2020). Automated detection of anthropogenic seismic noise in urban environments using
- machine learning. Seismological Research Letters **91**(4), 2453–2465.
- Herrera, M., L. Torgo, J. Izquierdo, and R. Pérez-García (2010). Predictive models for forecasting hourly urban water demand. *Journal of*
- 260 *hydrology* **387**(1-2), 141–150.
- Johnson, C. W., H. Meng, F. Vernon, and Y. Ben-Zion (2019). Characteristics of ground motion generated by wind interaction with trees,
- structures, and other surface obstacles. Journal of Geophysical Research: Solid Earth 124(8), 8519–8539.
- Jung, B. S., P. F. Boulos, D. J. Wood, and C. M. Bros (2009). A lagrangian wave characteristic method for simulating transient water column
- separation. Journal-American Water Works Association 101(6), 64–73.
- Kendrick, J., Y. Lavallée, T. Hirose, G. Di Toro, A. Hornby, S. De Angelis, and D. Dingwell (2014). Volcanic drumbeat seismicity caused by
- stick-slip motion and magmatic frictional melting. Nature Geoscience 7(6), 438-442.
- Larose, E., S. Carrière, C. Voisin, P. Bottelin, L. Baillet, P. Guéguen, F. Walter, D. Jongmans, B. Guillier, S. Garambois, et al. (2015).
- Environmental seismology: What can we learn on earth surface processes with ambient noise? Journal of Applied Geophysics 116,
- 269 62-74.
- Lecocq, T., S. P. Hicks, K. Van Noten, et al. (2020). Global quieting of high-frequency seismic noise due to covid-19 pandemic lockdown
- measures. Science **369**(6509), 1338–1343.
- Li, C., Z. Li, Z. Peng, C. Zhang, N. Nakata, and T. Sickbert (2018). Long-period long-duration events detected by the iris community
- wavefield demonstration experiment in oklahoma: Tremor or train signals? Seismological Research Letters 89(5), 1652–1659.
- Lindsey, N. J. and E. R. Martin (2021). Fiber-optic seismology. Annual Review of Earth and Planetary Sciences 49(1), 309–336.
- Lipovsky, B. and E. Dunham (2016). Tremor during ice-stream stick slip. *The Cryosphere* **10**(1), 385–399.
- ²⁷⁶ Maaten, L. v. d. and G. Hinton (2008). Visualizing data using t-sne. Journal of machine learning research 9(Nov), 2579–2605.
- Maher, S. P., M. E. Glasgow, E. S. Cochran, and Z. Peng (2025). Distinguishing natural sources from anthropogenic events in seismic data.
- 278 Seismological Research Letters **96**(1), 1–6.
- Massin, F., J. Farrell, and R. B. Smith (2013). Repeating earthquakes in the yellowstone volcanic field: Implications for rupture dynamics,
- ground deformation, and migration in earthquake swarms. Journal of volcanology and geothermal research 257, 159–173.
- Matoza, R. S., M. A. Garcés, B. A. Chouet, L. D'Auria, M. A. Hedlin, C. De Groot-Hedlin, and G. P. Waite (2009). The source of infrasound
- associated with long-period events at mount st. helens. Journal of Geophysical Research: Solid Earth 114(B4).
- 283 Matsuzawa, T., N. Uchida, T. Igarashi, T. Okada, and A. Hasegawa (2004). Repeating earthquakes and quasi-static slip on the plate boundary
- east off northern honshu, japan. Earth, planets and space **56**(8), 803–811.

- Meng, H. and Y. Ben-Zion (2018). Characteristics of airplanes and helicopters recorded by a dense seismic array near anza california.
- Journal of Geophysical Research: Solid Earth 123(6), 4783-4797.
- Nadeau, R. M. and L. R. Johnson (1998). Seismological studies at parkfield vi: Moment release rates and estimates of source parameters
- for small repeating earthquakes. Bulletin of the Seismological Society of America 88(3), 790-814.
- Nishida, K. (2017). Ambient seismic wave field. Proceedings of the Japan Academy, Series B 93(7), 423-448.
- Park, I., A. Jolly, K. Y. Kim, and B. Kennedy (2019). Temporal variations of repeating low frequency volcanic earthquakes at ngauruhoe
- volcano, new zealand. Journal of Volcanology and Geothermal Research 373, 108-119.
- Paul Winberry, J., S. Anandakrishnan, D. A. Wiens, and R. B. Alley (2013). Nucleation and seismic tremor associated with the glacial
- earthquakes of whillans ice stream, antarctica. Geophysical Research Letters 40(2), 312–315.
- Peng, Z. and J. Gomberg (2010). An integrated perspective of the continuum between earthquakes and slow-slip phenomena. Nature
- geoscience **3**(9), 599–607.
- Peng, Z. and X. Lei (2025). Physical mechanisms of earthquake nucleation and foreshocks: Cascade triggering, aseismic slip, or fluid flows?
- Earthquake Research Advances 5(2), 100349.
- Peng, Z., J. E. Vidale, A. G. Wech, R. M. Nadeau, and K. C. Creager (2009). Remote triggering of tremor along the san andreas fault in
- central california. *Journal of Geophysical Research: Solid Earth* **114**(B7).
- Poli, P., J. Boaga, I. Molinari, V. Cascone, and L. Boschi (2020). The 2020 coronavirus lockdown and seismic monitoring of anthropic
- activities in northern italy. *Scientific Reports* **10**(1), 9404.
- 302 Schwardt, M., C. Pilger, P. Gaebler, P. Hupe, and L. Ceranna (2022). Natural and anthropogenic sources of seismic, hydroacoustic, and
- infrasonic waves: Waveforms and spectral characteristics (and their applicability for sensor calibration). Surveys in Geophysics 43(5),
- 304 1265-1361.
- Shelly, D. R. (2024). Examining the connections between earthquake swarms, crustal fluids, and large earthquakes in the context of the
- 2020–2024 noto peninsula, japan, earthquake sequence. Geophysical Research Letters 51(4), e2023GL107897.
- Shelly, D. R., Z. Peng, D. P. Hill, and C. Aiken (2011). Triggered creep as a possible mechanism for delayed dynamic triggering of tremor
- and earthquakes. *Nature Geoscience* **4**(6), 384–388.
- 309 Si, X., X. Wu, H. Sheng, J. Zhu, and Z. Li (2024). Seisclip: A seismology foundation model pre-trained by multimodal data for multipurpose
- seismic feature extraction. IEEE Transactions on Geoscience and Remote Sensing 62, 1–13.
- St. Lawrence, W. and A. Qamar (1979). Hydraulic transients: A seismic source in volcanoes and glaciers. Science 203(4381), 654-656.
- Uchida, N. (2019). Detection of repeating earthquakes and their application in characterizing slow fault slip. *Progress in Earth and Planetary*
- 313 Science **6**(1), 1–21.
- Uchida, N. and R. Bürgmann (2019). Repeating earthquakes. Annual Review of Earth and Planetary Sciences 47(1), 305–332.
- Wang, X., E. F. Williams, M. Karrenbach, M. G. Herráez, H. F. Martins, and Z. Zhan (2020). Rose parade seismology: Signatures of floats
- and bands on optical fiber. Seismological Research Letters 91(4), 2395–2398.
- Winberry, J. P., S. Anandakrishnan, and R. B. Alley (2009). Seismic observations of transient subglacial water-flow beneath macayeal ice
- stream, west antarctica. Geophysical Research Letters **36**(11).

- Xiao, H., Z. C. Eilon, C. Ji, and T. Tanimoto (2020). Covid-19 societal response captured by seismic noise in china and italy. *Seismological*Society of America **91**(5), 2757–2768.
- Yin, A. (2018). Water hammers tremors during plate convergence. Geology 46(12), 1031–1034.
- Zhan, Z. (2020). Distributed acoustic sensing turns fiber-optic cables into sensitive seismic antennas. Seismological Research Letters 91(1),
- 323 1**-15**.
- ³²⁴ Zheng, Y. (2018). Transient pressure surge in a fluid-filled fracture. Bulletin of the Seismological Society of America 108(3A), 1481–1488.
- 252 Zheng, Y., H. Hu, F. J. Spera, M. Scruggs, G. Thompson, Y. Jin, T. Lapen, S. R. McNutt, K. Mandli, Z. Peng, et al. (2023). Episodic
- magma hammers for the 15 january 2022 cataclysmic eruption of hunga tonga-hunga ha'apai. Geophysical Research Letters 50(8),
- e2023GL102763.
- Zoet, L. K., S. Anandakrishnan, R. B. Alley, A. A. Nyblade, and D. A. Wiens (2012). Motion of an antarctic glacier by repeated tidally modulated earthquakes. *Nature Geoscience* **5**(9), 623–626.